

[1]

Radar-based short-term rainfall prediction

D.-J. Seo^{a,1} and J.A. Smith^{b,2}

^a*Hydrologic Research Laboratory, National Weather Service, NOAA, Silver Spring, MD 20910, USA*

^b*Department of Civil Engineering and Operations Research, Princeton University, Princeton, NJ 08544, USA*

(Received 27 December 1990; revised and accepted 30 May 1991)

ABSTRACT

Seo, D.-J. and Smith, J.A., 1992. Radar-based short-term rainfall prediction. *J. Hydrol.*, 131: 341–367.

A radar-based short-term rainfall prediction model is formulated and evaluated. The prediction lead time of interest is approximately 1 h. The model is composed of a physically based component and a statistical component. The physically based part performs mass balancing of mean vertically integrated liquid water content (VIL) under convective warm rainfall situations, using full-volume scan radar data, surface meteorological observations and upper air data. The statistical part performs prediction of residual VIL. Conversion of predicted VIL to rainfall is made using empirical relationships among VIL, rainwater content at cloud bottom, and echo-top height, which is assumed to remain constant over the prediction lead time.

To evaluate the model, a comparison is made against advection-based nowcasting using radar data from the National Weather Service Radar Data Processor, version II (RADAP II) system at Oklahoma City. Results from parameter estimation runs show that inclusion of the simple physical and statistical dynamics has potential in improving advection-based nowcasting under convective situations. An apparent bias in mean rainfall prediction, however, suggests room for improvement. Issues concerning possible improvements are described, and future research directions are discussed.

INTRODUCTION

A characteristic feature of flash floods is that the lead time available for warning is quite short. For example, in the Shadyside, Ohio, USA, flash flood of June 1990, loss of life occurred within 1 h of onset of rainfall. Because of the short lead times involved, short-term rainfall prediction is an integral component of flash flood forecasting systems (Saffle and Greene, 1978; Huff and Vogel, 1981; Einfalt et al., 1990).

¹ Present address: Systems Engineering Research Institute, Korea Institute of Science and Technology, Daejeon, South Korea 305-600.

² Author for correspondence.

Short-term prediction of rainfall has been studied by a number of authors. Johnson and Bras (1980) developed statistical prediction procedures using rain gage observations. In a similar vein, Georgakakos and Bras (1984a,b) developed procedures using surface meteorological observations as well as rain gage observations. An important feature of the procedures of Georgakakos and Bras (1984a,b) is that physical arguments are used in deriving model structure. Browning and Collier (1989) reviewed a broad class of procedures known as 'nowcasting' or projection procedures. Projection procedures have been widely used with radar rainfall data (Elvander, 1976; Bellon and Austin, 1978, 1984; Browning et al., 1982; Walton and Johnson, 1986; Einfalt et al., 1990). The essence of projection procedures is that the current rainfall pattern (or storm elements within the rainfall pattern) is projected spatially using an advection velocity derived from the recent time history of rainfall. Little attention has been given, however, to combining projection procedures with simple dynamic models which utilize meteorological observations from surface and upper air stations, and radar rainfall data.

New technologies in the United States will greatly expand the potential for short-term rainfall prediction. A network of more than 120 weather radars, the Next Generation Weather Radar (NEXRAD) system, is expected to be deployed over the period 1991–1995. Also a new communications and processing system, the Automated Weather and Interactive Processing System (AWIPS), will combine radar and meteorological observations with modern computer processing power. In this paper we develop procedures that can exploit these new technologies. In particular, we investigate the potential for improving projection-type rainfall predictions over a time scale of 1 h by incorporating simple physical and statistical dynamics components.

We assume that the vertically integrated liquid water (VIL) field of a rainfall system at time t can be decomposed spatially into a slowly varying mean field and a rapidly varying residual field:

$$VI_t(i, j) = AV_t + RE_t(i, j) \quad (1)$$

where $VI_t(i, j)$ is the VIL at (i, j) th radar bin at time t , AV_t is the local mean VIL at time t , $RE_t(i, j)$ is the residual VIL at (i, j) th radar bin at time t . The idea then is to predict $AV_{t+\Delta t}$ and $RE_{t+\Delta t}(i + \Delta i, j + \Delta j)$ using physical and statistical models, respectively, and convert predicted $VI_{t+\Delta t}(i + \Delta i, j + \Delta j)$ to rainfall, where Δi and Δj denote the advection distances in time Δt along x and y directions, respectively. The physical model performs mass balancing of VIL using full-volume scan radar data, hourly surface observations and radiosonde data. The residual model performs prediction of residual VIL. The models are formulated in a Lagrangian framework, that is, our coordinate system moves with the advection of the rainfall system.

The size of a radar bin is chosen to be the size of a Hydrologic Rainfall Analysis Project (HRAP) (Greene and Hudlow, 1982) bin, which is approximately $4 \times 4 \text{ km}^2$ for the study area encompassing Oklahoma City. The size of the area over which the local mean is computed depends largely on the density of the meteorological observation networks. In this work, we used an averaging area of approximately $12 \times 12 \text{ km}^2$ (three HRAP bins on a side).

In the following sections, we describe the physically based model, estimation of VIL, estimation of saturation vapor density, estimation of updraft velocity, residual prediction, verification, results, and conclusions and future research recommendations.

PHYSICALLY BASED MODEL

The physically based model performs a mass balancing of VIL under convective warm rainfall situations. It uses: (1) radar volume scan data to estimate the initial VIL; (2) surface measurements of temperature, pressure and dew point temperature to estimate profiles of in-cloud temperature and saturation water vapor density; (3) radiosonde data to obtain profiles of environmental temperature and water vapor density. Many of the developments below closely follow those of Kessler (1969).

To obtain the mass balance equation for VIL, we start with the following continuity equations for rainwater content, cloudwater content, saturation water vapor density and density of air:

$$\frac{\partial M}{\partial t} + \frac{\partial(Mu)}{\partial x} + \frac{\partial(Mv)}{\partial y} + \frac{\partial[M(w + V)]}{\partial z} = 0 \quad (2)$$

$$\frac{\partial m}{\partial t} + \frac{\partial(mu)}{\partial x} + \frac{\partial(mv)}{\partial y} + \frac{\partial(mw)}{\partial z} = 0 \quad (3)$$

$$\frac{\partial Q}{\partial t} + \frac{\partial(Qu)}{\partial x} + \frac{\partial(Qv)}{\partial y} + \frac{\partial(Qw)}{\partial z} = 0 \quad (4)$$

$$\frac{\partial \rho}{\partial t} + \frac{\partial(\rho u)}{\partial x} + \frac{\partial(\rho v)}{\partial y} + \frac{\partial(\rho w)}{\partial z} = 0 \quad (5)$$

where M is the rainwater content, m is the cloudwater content, Q is the saturation water vapor density, ρ is the density of air, V is the fall velocity of the rain water, and u , v and w are the velocities of air in x , y and z directions, respectively. Rain and cloudwater content, like saturation vapor density, are represented as mass per unit volume. Cloud water is different from rain water in that cloud water follows the motion of air. In this work, we limit ourselves to warm rainfall processes only, and thus no phase change is allowed. Under

the assumptions of locally steady and horizontally uniform saturation vapor density and incompressible air, eqns. (3) and (4) may be added to yield:

$$\frac{\partial m}{\partial t} = -w \frac{\partial m}{\partial z} - w \frac{\partial Q}{\partial z} \quad (6)$$

Also, under the assumption of incompressible air, eqn. (2) can be rewritten as:

$$\frac{\partial M}{\partial t} = -w \frac{\partial M}{\partial z} - \frac{\partial(MV)}{\partial z} \quad (7)$$

In eqns. (6) and (7), terms involving u and v are omitted since we are adopting the Lagrangian coordinate system which follows the advection of the rainfall system. In this formulation, lateral mixing is ignored. It can be justified in this work because vertical flux should dominate mass balancing given the large averaging area of about $12 \times 12 \text{ km}^2$.

Equations (6) and (7) are still difficult to work with because radar, in general, does not distinguish cloud water from rain water. For example, most 10 cm radars begin to show an echo when drops exceed $200 \mu\text{m}$ in diameter (Simpson and Wiggert, 1969). To circumvent this difficulty, we assume that, on condensation, water vapor is immediately converted to rain water without first forming cloud water. Then eqns. (6) and (7) may be added to yield:

$$\frac{\partial M}{\partial t} = -w \frac{\partial M}{\partial z} - \frac{\partial(MV)}{\partial z} - w \frac{\partial Q}{\partial z} \quad (8)$$

Another interpretation which leads to eqn. (8) is that cloudwater content is steady state and has a uniform profile. Both assumptions certainly limit the applicability of eqn. (8). Treating cloudwater content as a separate state variable, however, greatly complicates the problem in that (1) cloudwater content cannot be estimated using a conventional weather radar, and (2) one has to include various microphysical processes between cloud water and rain water such as coalescence, collision, breakup, evaporation, etc. In this work, we assume that liquid water content, as estimated from radar data, consists of rain water only. Equation (8) can be integrated from cloud bottom, z_B , to echo-top, z_T , to yield the following mass balance equation for VIL:

$$\frac{d\bar{M}}{dt} = w_B M_B + \int_{z_B}^{z_T} \frac{dw}{dz} M dz + M_B V_B + w_B Q_B - w_T Q_T + \int_{z_B}^{z_T} \frac{dw}{dz} Q dz \quad (9)$$

$$\bar{M} = \int_{z_B}^{z_T} M dz \quad (10)$$

where w_B and w_T are the updraft velocities at cloud bottom and at echo-top, respectively, M_B is the rainwater content at cloud bottom, V_B is the fall velocity of rain water at cloud bottom, and Q_B and Q_T are the saturation water vapor densities at cloud bottom and at echo-top, respectively. In obtaining eqn. (9), we used the Leibniz rule and integration by parts. Also used are the assumptions that rainwater content at echo-top is zero and cloud bottom elevation remains constant over the prediction lead time. Rainfall accumulation at z_B from t_0 to t_1 , for example, is then given by:

$$P_B = \int_{t_0}^{t_1} q_B(x + u\tau, y + v\tau, \tau) d\tau \tag{11a}$$

$$= - \frac{1}{\rho_w} \int_{t_0}^{t_1} (w_B + V_B)M_B dt \tag{11b}$$

where $q_B(x, y, t)$ denotes the rainfall rate at altitude z_B at location (x, y) at time t , and ρ_w is the density of rain water.

Because we are not solving a vertical momentum equation along with eqn. (8), w_B and w_T must be specified externally. Kessler (1969) assumed that updraft velocity profile remains constant over the prediction lead time and can be represented as a quadratic function of altitude. Even with such a simplifying assumption, eqn. (9) is still difficult to work with as it would involve terms such as

$$\int_{z_B}^{z_T} zM dz$$

Equation (8) pertains to the mass balancing of VIL over an area larger than the radius of a typical updraft column. When averaged over a relatively large area, updraft profile should be characterized by a much smaller gradient than that within an individual updraft column. Also, as will be seen in the next section, z_B in this work is taken not at the cloud bottom, or at the lifting condensation level (LCL), but at a relatively high altitude of 2.5 km for validation purposes. It is then, reasonable to assume that updraft profile between z_B and z_T is approximately uniform. Equation (9) is then reduced to:

$$\frac{d\bar{M}}{dt} = (w_m + V_B)M_B + w_m(Q_B - Q_T) \tag{12}$$

where w_m is the average updraft velocity. The interpretation of eqn. (12) is simply that the time rate of change in VIL is the sum of net outflux of rain water through z_B and net influx of water vapor between z_B and z_T . Time-integrated versions of mass balance equations similar to eqn. (12) have been used in diagnostic studies of radar observations of precipitation production in thunderstorms (Reuter, 1990, see also references therein).

Under the assumption of Marshall-Palmer raindrop size distribution (Marshall and Palmer, 1948), V_B in eqn. (12) can be determined easily. A packet of rain water with content M is assumed to fall with velocity V . It is easy to show that V is given by the following:

$$V = -a[\Gamma(4 + b)/6](\pi\rho_w N_0)^{-b/4} M^{b/4} \quad (13)$$

where a and b are the constant and the exponent, respectively, in the terminal velocity-drop diameter relationship of Gunn and Kinzer (1949)

$$V_t(D) = -aD^b$$

$\Gamma(t)$ denotes the Gamma function, and N_0 is the parameter in the Marshall-Palmer raindrop size distribution,

$$n(D) = N_0 e^{-\lambda D}$$

In the following sections, we describe how the remaining variables in eqn. (12) are determined.

ESTIMATION OF VIL

The radar data used in this work are from the Radar Data Processor, version II (RADAP II) system at Oklahoma City. The radar is a WSR-57 and has a wavelength of 10 cm and a beam width of 2.2° . Radial and vertical sampling points are illustrated in Fig. 1, each point representing the center of the sampling volume. The radials are centered on even azimuths. Elevation angles corresponding to the beams in Fig. 1 are 0.5, 2, 4, 6, 8, 10, 12, 14, 16.

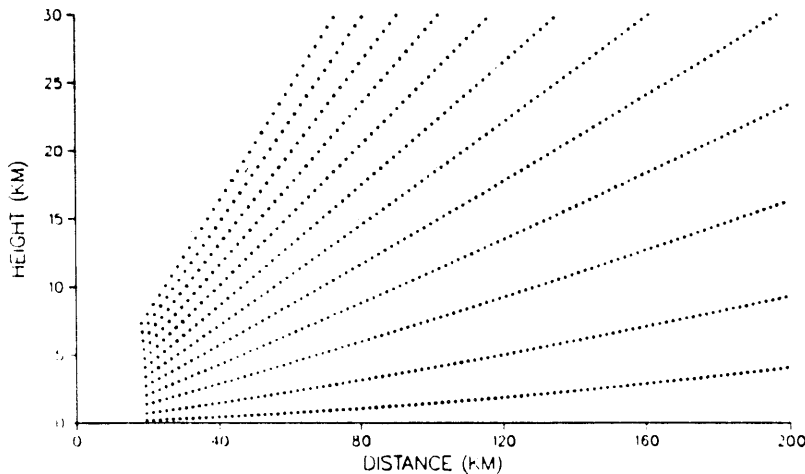


Fig. 1. Centers of sampling volumes in RADAP II at each azimuth.

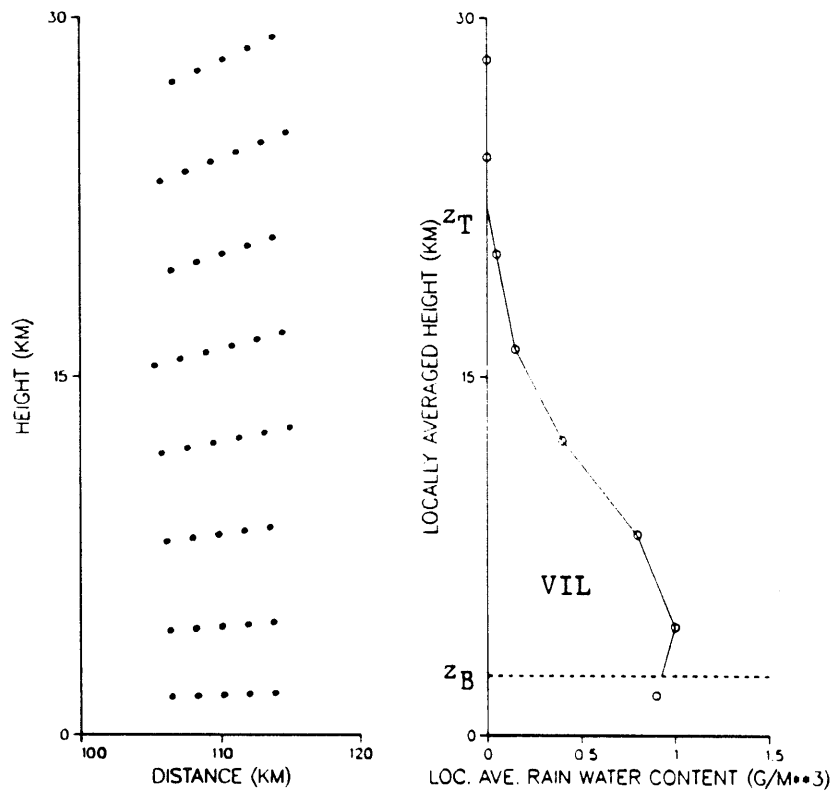


Fig. 2. One-dimensional schematic of VIL estimation.

20, and 22°. Figure 2 illustrates a one-dimensional schematic of how VIL would be computed over a $10 \times 10 \text{ km}^2$ column. In many cases, it was not possible to obtain VIL, typically for the following reasons: (1) higher elevation beams were lacking so that echo-top height could not be determined; (2) the number of data points was too small at the outer rim of the radar umbrella. Owing to the various types of errors involved, it is difficult to assess the accuracy of estimated VIL. In this work, we used only radar data within a radius of 160 km from the radar site. Even with this reduced areal coverage, the vertical sampling interval at the outermost rim is very large (about 3 km). Further reduction of areal coverage, however, would yield too small a sample size to work with.

A natural way of specifying z_B would be as the lifting condensation level (LCL). LCL, however, can be very low and may not be well sampled by the lowest radar beam of 0.5 degrees of elevation angle. Also, near the radar site, radar data from lower beams are likely to be affected by ground clutter. For these reasons, we set z_B at 2.5 km.

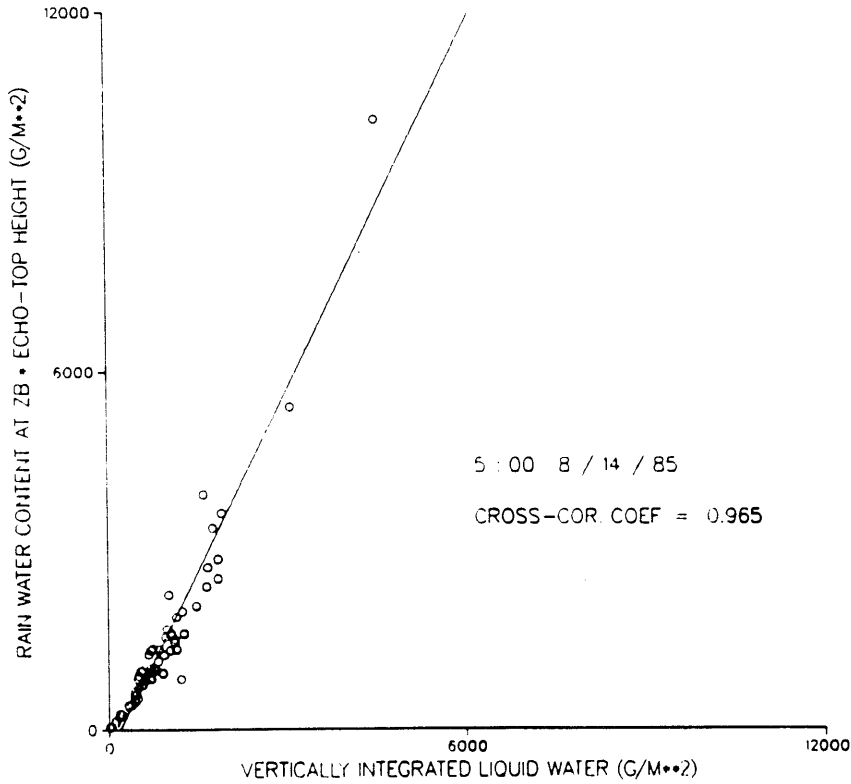


Fig. 3. Example scatter plot of $M_B H$ and \bar{M} , and the linear fit.

As we vertically integrated eqn. (8), as opposed to solving it directly, M_B remains undetermined in eqn. (12). M_B is trivially determined only when the vertical profile of rainwater content remains uniform or triangular under the assumption of constant echo-top height over the prediction lead time. As a compromise, we assumed in this work that, over the prediction lead time: (1) echo-top height remains constant; (2) the following relation holds among M_B , \bar{M} and the constant echo-top height:

$$M_B = (a_1 \bar{M} + a_0) / H \quad (14)$$

where H is the echo-top height above z_B ($= z_T - z_B$), and a_1 and a_0 are coefficients estimated via least squares fit using the estimates of M_B , H and \bar{M} , obtained from the most recently available full-volume scan data. In many cases, scatter plots between $M_B H$ and \bar{M} suggest that a quadratic fit or a square root fit might be somewhat better. In this work, however, we used a linear fit throughout for simplicity. Figure 3 shows an example scatter plot and the best fit.

ESTIMATION OF SATURATION VAPOR DENSITY

Vertical profile of saturation vapor density was estimated assuming adiabatic lifting of a parcel from the ground to LCL and moist-adiabatic lifting of the parcel with entrainment from LCL to the echo-top. Under the assumption of hydrostatic atmosphere, adiabatic and moist-adiabatic lapse rates are given as follows (Hess, 1979):

from surface to LCL

$$-\frac{\partial T}{\partial z} = \frac{g}{c_p} \quad (15)$$

from LCL to echo-top

$$-\frac{\partial T}{\partial z} = \frac{\frac{g}{c_p} \left[1 + \frac{L_{iv} r_s}{R_d T} \right] + \mu \left[(T - T_e) + \frac{L_{iv}}{c_p} (r_s - r_e) \right]}{1 + \frac{L_{iv}^2 r_s}{c_p R_v T^2}} \quad (16)$$

where z is the geopotential height in m, T is the temperature inside the cloud at z in K, g is the gravitational acceleration in m s^{-2} , c_p is the specific heat in $\text{J g}^{-1} \text{K}$, L_{iv} is the latent heat of vaporization of water in J g^{-1} , R_d is the gas constant for dry air in $\text{J g}^{-1} \text{K}$, r_s is the saturation mixing ratio inside of the cloud at z in g g^{-1} , μ is the entrainment rate per unit height in m^{-1} , T_e is the environmental temperature at z in K, r_e is the environmental mixing ratio at z in g g^{-1} and R_v is the gas constant for moist air in $\text{J g}^{-1} \text{K}$ ($= 1.61 R_d$). The saturation mixing ratio r_s is given by (Dutton, 1986):

$$r_s = 0.621 e_s / (p - e_s) \quad (17)$$

where e_s is the saturation vapor pressure at z in mbar, and p is the pressure at z in mbar, assumed to be the same both inside and outside the cloud. The saturation vapor pressure e_s is given by (Dutton, 1986):

$$e_s = 6.11 \exp [(L_{iv}/R_v)(1/273 - 1/T)] \quad (18)$$

The pressure p is determined via the hydrostatic approximation for moist air (Dutton, 1986):

$$\partial p / \partial z = -10^{-5} g \rho_d (1 + r_e) \quad (19)$$

where ρ_d is the density of dry air in g m^{-3} .

To solve eqn. (16), we need to know T at LCL, and profiles of T_e and r_e . Given temperature, dew point temperature, and pressure at the surface, LCL can be computed under the hydrostatic assumption (see, for example,

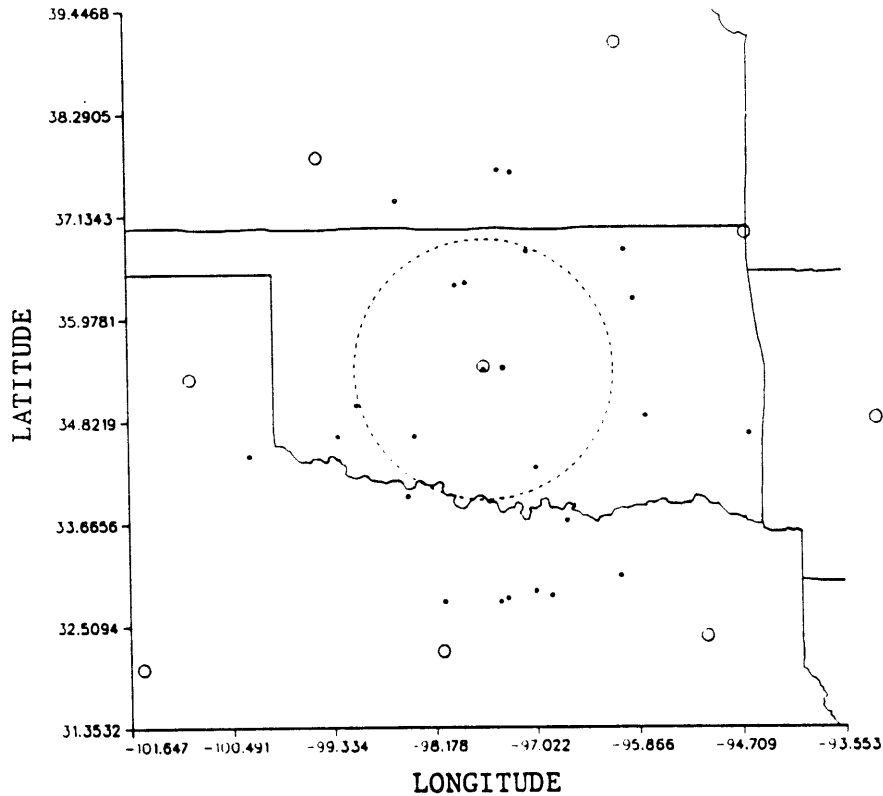


Fig. 4. Map of study area. The reduced radar umbrella, centered at Oklahoma City, is the model domain. Small solid circles denote rain gage location. Large empty circles denote radiosonde sites.

Pruppacher and Klett, 1978). In this work, surface measurements of temperature, dew point temperature and pressure were obtained from a network of surface stations shown in Fig. 4 as small solid circles. For those grids which included a surface station, the point measurements at the station were used as representative of the spatially averaged condition at the surface. For those grids which did not include a surface station, an interpolation was performed using measurements from the three nearest surface stations. The interpolation involved two steps. The first was to adjust, under the hydrostatic assumption, measurements of temperature and dew point temperature at each of the three nearest stations to the pressure level at the grid surface, by lifting or lowering a parcel adiabatically or moist-adiabatically from the ground level of the station to that of the grid (see, for example, Georgakakos and Bras, 1984a,b). The second involved the inverse distance weighting of the three adjusted measurements (Pielke, 1984).

The environmental temperature T_e and the environmental mixing ratio r_e were obtained from a network of radiosonde observations shown in Fig. 4 as

large empty circles. In this work, we used measurements of T_c and r_c at pressure levels with increments of 50 mbar from 1000 to 50 mbar. Profiles of T_c and r_c at an arbitrary grid within the model domain were then reconstructed by performing the inverse distance weighting of the three nearest radiosonde observations at each pressure level. In this work, we used the latest sounding at 12:00 or 00:00 GMT prior to the start of prediction. Once prediction was started, however, the initial sounding was assumed to persist throughout the duration of the storm. Use of a new sounding, which may become available during the duration of the storm, may result in an abrupt change in estimated updraft velocity (see the next section), and thus was avoided.

The saturation water vapor densities at z_B and z_T , Q_B and Q_T , respectively, in eqn. (12) are then obtained from:

$$Q_B = 10^2 r_{sB} p_B / (R_d T_B) \quad (20)$$

$$Q_T = 10^2 r_{sT} p_T / (R_d T_T) \quad (21)$$

where Q_B and Q_T are in g m^{-3} , r_{sB} and r_{sT} are the saturation mixing ratios at z_B and z_T in g g^{-1} , respectively, p_B and p_T are the pressures at z_B and z_T in mbar, respectively, and T_B and T_T are the temperatures inside of the cloud in K at z_B and z_T , respectively. In obtaining eqns. (20) and (21), we used the approximation of eqn. (17) and the ideal gas law for water vapor.

ESTIMATION OF UPDRAFT VELOCITY

The average updraft velocity w_m was estimated using the one-dimensional cloud model of Simpson and Wiggert (1969) under the assumption of locally steady updraft:

$$\frac{1}{2} \frac{\partial w^2}{\partial z} = \frac{g}{1 + \gamma} \frac{T_v - T_{ve}}{T_{ve}} - g r_{lw} - \mu w^2 \quad (22)$$

where w is the updraft velocity at z in m s^{-1} , γ is the virtual mass coefficient, T_v is the in-cloud temperature in K, T_{ve} is the temperature of the environmental air in K, and r_{lw} is the mixing ratio of the liquid water in the cloud in g g^{-1} . The entrainment rate μ is related to the radius of the cloud through the experimental relationship $\mu = 0.183/R_c$, where R_c is the radius of the cloud (Anthes, 1977). In this work, we omitted r_{lw} (and thus the effect of water load) as we did not know the cloudwater content. Given the vertical profiles of T_v , T_{ve} and r_{lw} , eqn. (22) could be solved, with the boundary condition that updraft velocity at the surface is zero, to give:

$$w = \left\{ 2 \int_{z_0}^z \left[\frac{g}{1 + \gamma} \frac{T_v - T_{ve}}{T_{ve}} - g r_{lw} \right] e^{-2\mu(z-u)} du \right\}^{1/2} \quad (23)$$

where z_0 is the height at the surface.

As noted earlier, we assumed that between z_B and z_T , updraft profile is approximately uniform. In this work, we used eqn. (23) to obtain only the maximum updraft velocity, w_{\max} , by taking the upper bound to be the height where buoyancy becomes negative. Note that, if there is no entrainment, w_{\max}^2 thus obtained is essentially the energy of instability (Dutton, 1986). As w_m in eqn. (12) is only a fraction of w_{\max} , we assumed:

$$w_m = kw_{\max} \quad (24)$$

where k is a constant whose value ranges from 0 to 1. Both the entrainment rate μ (or, the radius of cloud R_c) and the constant k are model parameters to be estimated. In interpreting estimated values of μ or R_c , it is understood that they are viewed as characteristic entrainment rate or radius of cloud, representative of the average condition over the whole rainfall field, rather than pertaining to individual clouds.

RESIDUAL PREDICTION

The physically based model describes dynamics of VIL over a relatively large area (about $12 \times 12 \text{ km}^2$ in this work). In an effort to capture smaller scale features, a residual prediction procedure was introduced. We assume that residual VIL follows the frozen field model (Callahan et al., 1982; Gupta and Waymire, 1988) of the following form:

$$dR_{vi}/dt = \alpha R_{vi} + Z \quad (25)$$

where R_{vi} is the residual VIL, α is the friction coefficient, and Z is assumed to be the zero-mean white noise in space and time. Although the white noise assumption is certainly an oversimplification, the margin of improvement by using a more complicated statistical model is considered relatively small. Equation (25) is then equivalent to the autoregressive-1 model, and thus, for $k = 1, 2, 3, \dots$, we have:

$$E[RE_{t+k \times \Delta t}(i+k \times \Delta i, j+k \times \Delta j) | RE_t(i, j)] = c^k RE_t(i, j) \quad (26)$$

where c is the lag - 1 Lagrangian autocorrelation coefficient. In eqn. (26), Δi and Δj are displacements, in units of radar bins, along x and y directions, respectively, during a time interval of duration Δt . In this work, Δt was taken to be 10 min, the smallest interval between two consecutive sets of full-volume scan data for RADAP II. Following eqn. (1), the predicted VIL is given by:

$$\bar{V}I_{t+k \times \Delta t} = E[VI_{t+k \times \Delta t}(i+k \times \Delta i, j+k \times \Delta j) | VI_t(i, j)] \quad (27a)$$

$$= AV_{t+k \times \Delta t} + c^k RE_t(i, j) \quad (27b)$$

Conversion of $\bar{V}I_{t+k \times \Delta t|t}$ to rainfall at z_B amounts to specifying rainwater content at z_B at $(i + k \times \Delta i, j + k \times \Delta j)$ th radar bins for all k . The conversion was made following the same approach used in relating \bar{M} and M_B , i.e.

$$\bar{M}B_{t+k \times \Delta t|t} = (b_1 \bar{V}I_{t+k \times \Delta t|t} + b_0)/h \tag{28}$$

where $\bar{M}B_{t+k \times \Delta t|t}$ is the predicted rainwater content at z_B at $(i + k \times \Delta i, j + k \times \Delta j)$ th bin, h is the echo-top height above z_B at (i, j) th bin at time t , assumed to be constant over the prediction lead time, and b_1 and b_0 are coefficients estimated via least squares fit using the estimates of VIL, rainwater content at z_B and echo-top height above z_B , obtained from the full-volume scan data at time t . Figure 5 shows an example scatter plot and the best fit.

A discrete approximation to the rainfall accumulation at z_B over the prediction lead time of $n \times \Delta t$ (eqn. (11a,b)), may then be obtained from:

$$P_B \approx \frac{1}{\rho_w} \sum_{k=0}^{n-1} \{a[\Gamma(4 + b)/6](\pi\rho_w N_0)^{-b/4} \bar{M}B_{t+k \times \Delta t|t}^{1+b/4} - w_m \bar{M}B_{t+k \times \Delta t|t}\} \Delta t \tag{29}$$

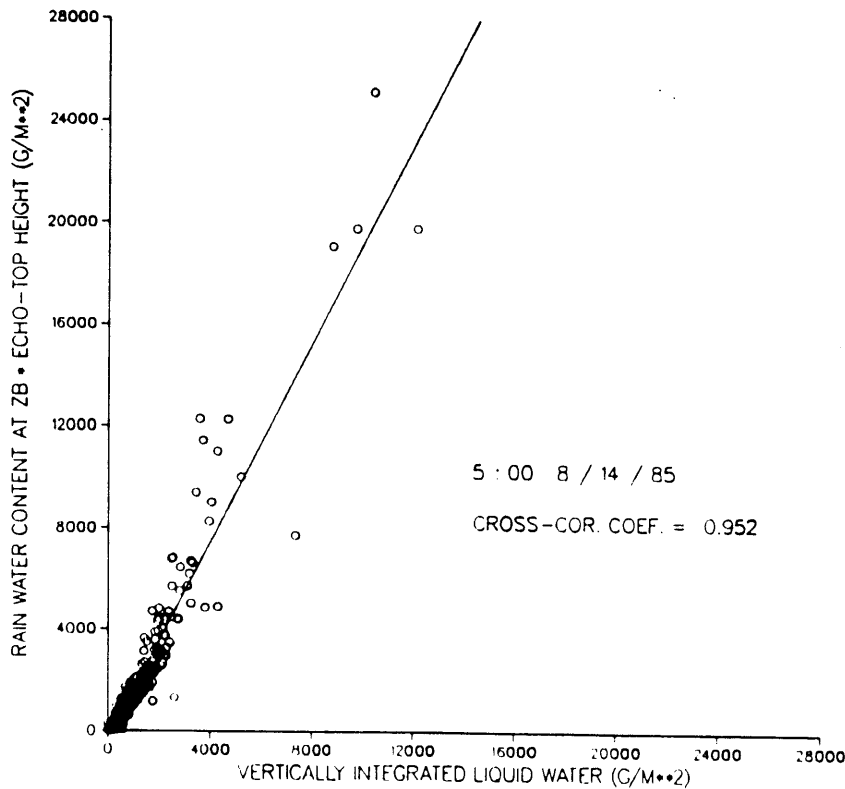


Fig. 5. Example scatter plot of $\bar{M}B, h$ and $\bar{V}I_t$, and the linear fit.

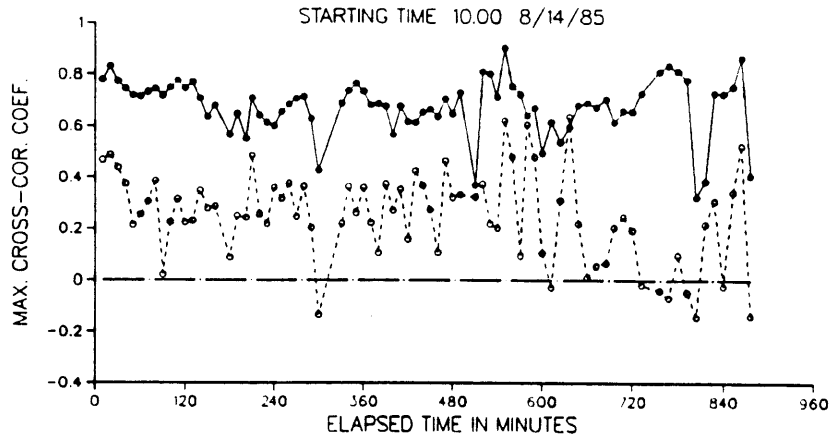


Fig. 6. Example time series plots of maximum cross-correlation coefficient of VIL (solid circles connected with solid lines) and the corresponding cross-correlation coefficient of residual VIL (open circles connected with dashed lines).

Ideally, we would like to obtain conditional expectation of rainfall accumulation at time $t + k \times \Delta t$ given $RE_i(i, j)$. As P_B is not linear in $\bar{M}B_{t+k \times \Delta t}(t)$, P_B is not the conditional expectation. Given the whole host of assumptions and approximations, however, P_B is a reasonable approximation.

Estimation of the Lagrangian autocorrelation coefficient of residual VIL at lag Δt , c , involves estimation of advection velocity. In this work, advection velocity is estimated by computing the cross-correlation field between two consecutive VIL fields, and locating the maximum. The technique is described by Leese et al. (1971), and is not detailed here. It is noted that, since advection velocity is external to the model, we may adopt other, potentially better, techniques for advection velocity estimation.

For RADAP II, full-volume scan data are available every 10 or 12 min, and thus the maximum cross-correlation vector was computed every 10 or 12 min. Figure 6 shows an example of the time series of maximum cross-correlation coefficient (i.e. Lagrangian autocorrelation coefficient) of VIL (solid circles connected with solid lines). The lag time corresponding to a datum of correlation coefficient in Fig. 6 is given by the time elapsed from the immediately preceding datum. The six or five displacement vectors obtained were then summed to represent the advection velocity in the hour. The Lagrangian autocorrelation coefficient of residual VIL, c , is then given by the cross-correlation coefficient between the two consecutive residual VIL fields. Magnitude of c depends also on the size of the averaging area: a larger averaging area will generally result in a larger c , and vice versa. Figure 6 shows an example of the time series of maximum cross-correlation coefficient of residual VIL (empty circles connected with dashed lines).

VERIFICATION

Probably the best way to validate model performance would be to compare predicted rainfall against a combination of measurements from a dense network of rain gages and radar data. Such a dense rain gage network, however, does not exist in the study area. The quality of readily available hourly rain gage measurements is not suitable for detailed comparison with radar data (time-synchronization is a particularly common problem; see Seo and Smith 1991). For these reasons, we resorted exclusively to radar data for validation purposes. The crucial assumption behind this was that bias in the radar-derived rainfall or rainwater content, if it existed, remained constant over the duration of each storm. If suitable rain gage data had existed, some form of bias correction could have been performed (see, for example, Smith and Krajewski, 1991). It is known (Seo and Smith, 1991) that there is little long-term bias in the RADAP II-derived rainfall at Oklahoma City. Given the limited number of rain gage data, however, it was not possible to examine changes in bias over the duration of a single storm.

Under the assumption of Marshall–Palmer raindrop size distribution, Gunn–Kinzer raindrop size-terminal velocity relationship and no updraft, it is easy to show that reflectivity factor, rainwater content and rainfall rate are related as follows:

$$Z = 10^{18} N_0 \lambda^{-7} \Gamma(7) \quad (30)$$

$$M = 10^6 \pi N_0 \lambda^{-4} \quad (31)$$

$$R = 6^5 \pi a N_0 \lambda^{-(4+b)} \Gamma(4 + b) \quad (32)$$

where Z is the reflectivity factor in $\text{m}^6 \text{m}^{-3}$, N_0 is the parameter in the M – P distribution in $\text{m}^{-3} \text{m}^{-1}$, λ^{-1} is the mean diameter in m , $\Gamma(t)$ is the Gamma function, M is the rainwater content in gm^{-3} , R is the rainfall rate in mm h^{-1} , and a and b are the constant and the exponent in the dropsize-fall velocity relationship (dropsize in m and fall velocity in m s^{-1}) of Gunn and Kinzer type. In this work, we used $a = 130$ and $b = 0.5$ following Kessler (1969), which yields:

$$Z = 206 R^{14/9} \quad (33)$$

$$M = 3.44 \times 10^{-3} Z^{4/7} \quad (34)$$

$$R = 19.2 M^{1.125} \quad (35)$$

With eqn. (35), prediction of rainfall at z_B amounts to prediction of rainwater content at z_B under no updraft. A discrete approximation to the rainfall accumulation in mm at z_B over the prediction lead time of an hour ($n = 6$ and

TABLE 1

Starting and ending time (in GMT) of storm cases, and optimal parameter values

Case number	Starting hour	Ending hour	No. of hours	Optimal R_c (km)	Optimal k
1	21 08/05/85	3 08/06/85	7	5.0	0.40
2	1 08/14/85	7 08/14/85	7	3.0	0.10
3	23 07/17/87	4 07/18/87	6	7.5	0.60
4	8 09/27/87	17 09/27/87	10	25.0	0.05
5	18 06/26/88	1 06/27/88	8	10.0	0.10
6	22 08/09/88	7 08/10/88	10	10.0	0.20
7	4 09/03/88	11 09/03/88	8	10.0	0.05

$\Delta t = 10$ min) is then given by:

$$P_B \approx 19.2 \sum_{k=0}^{n-1} [b_1 \bar{V} I_{t+k \times \Delta t} + b_0]^{1.125} \Delta t \quad (36)$$

From the archive of Oklahoma City RADAP II data, a total of seven storm cases, each lasting several hours or longer, were selected (see Table 1). The selection process was severely limited by many missing data particularly when heavy rainfall was occurring. From 1985 through 1988, a total of only 12 cases, each lasting several hours, was selected. We then examined the daily weather maps from the National Oceanic and Atmospheric Administration (NOAA), and excluded five frontal cases.

Because of the small number of storm cases, it was not possible to perform both parameter estimation and validation using independent data sets. The results given in the next section are based on the parameter values that were tuned to yield the best prediction under the criteria of minimum root mean square error and mean error. Also, when prediction was made at the beginning of hour i , advection components, u and v , for that hour were obtained not from the vector sum of advection vectors in the preceding hour, but from that in the current hour for parameter estimation purposes. For comparison purposes, we included nowcasting based solely on the advection of the instantaneous rainfall field at the altitude of 2.5 km observed by radar at the time of prediction. The advection vector used in nowcasting was exactly the same as that used in the model prediction. Therefore, model prediction differs from nowcasting only in that it includes physical and statistical dynamics.

RESULTS

The two parameters, R_c and k , were estimated by locating the optimal combination which yielded the minimum root mean square error and absolute

MEAN ERROR

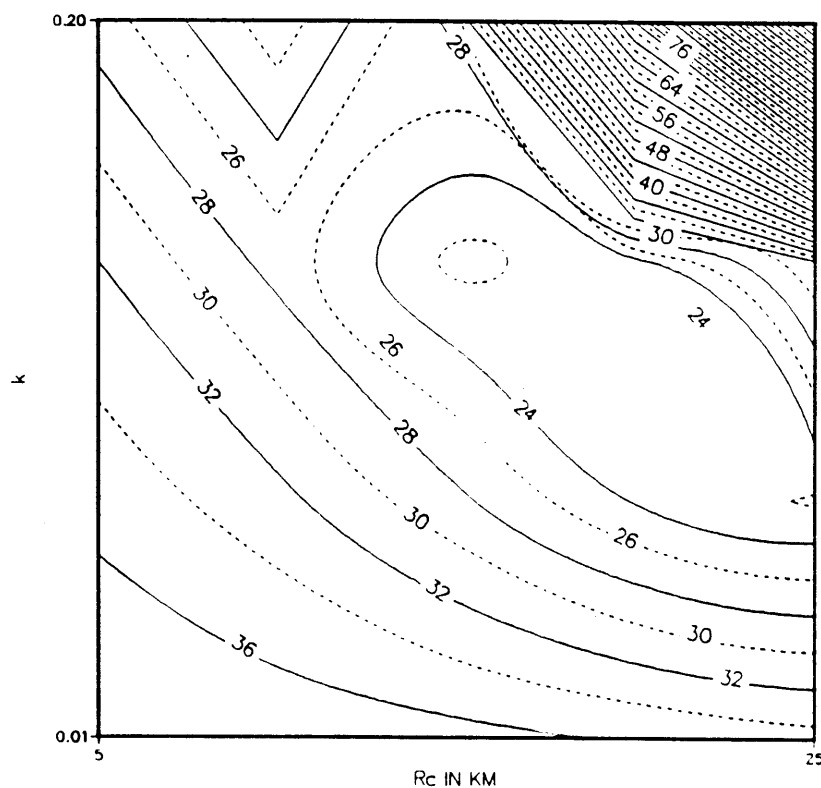


Fig. 7. Mean error on the $R_c - k$ space.

mean error on the $R_c - k$ space over the duration of each storm case. As R_c and k are generally time-varying parameters, they will have to be estimated in real time. In this work, given the limited data, we assumed that the parameter values remained constant for the duration of each storm case. Figures 7 and 8 show examples of absolute mean error and root mean square error on the parameter space. Most of the cases yielded a clear optimum.

Figures 9-15 show the mean rainfall and root mean square error (r.m.s.e.) of cases 1-7, respectively, over the duration of the storm. Crosses connected with chain-dotted lines pertain to hourly radar rainfall fields, assumed to be the true hourly rainfall fields. Empty circles connected with dashed lines pertain to advection-based nowcast hourly rainfall fields. Solid circles connected with solid lines pertain to model-predicted hourly rainfall fields. Missing statistics in the figures are due to missing scans and lack of higher vertical scans in computing VIL. Also shown below the x axis name at each

ROOT MEAN SQUARE ERROR

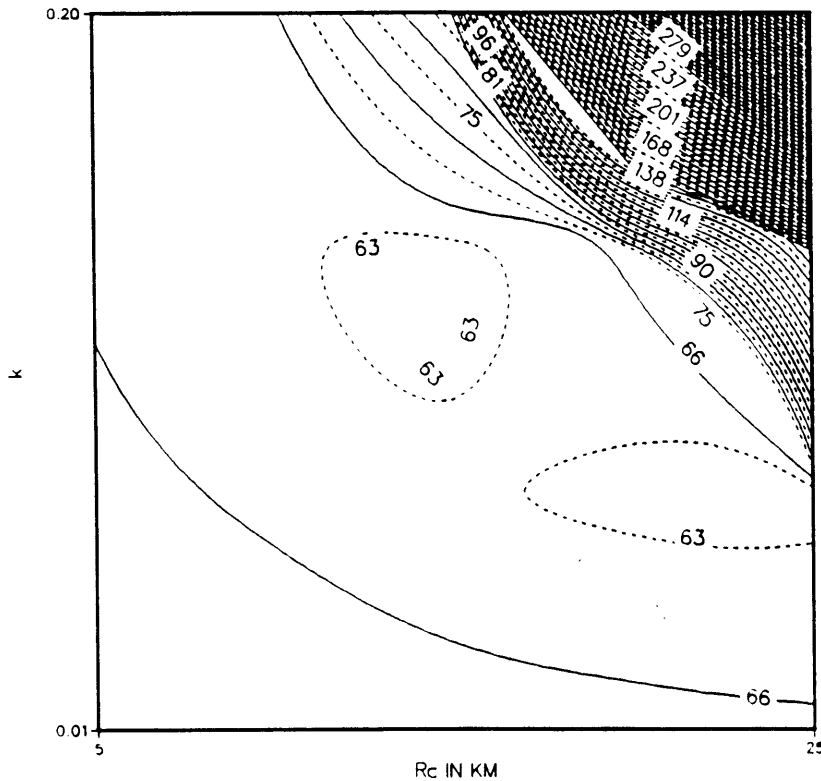


Fig. 8. Root mean square error on the $R_c - k$ space.

hour is the number of data points used to compute the statistics. Figures 16–18 show examples of radar rainfall field at the altitude of 2.5 km, used as true rainfall field at that altitude, predicted rainfall field and nowcast rainfall field at the same altitude, respectively. A 'bar' symbol indicates that model prediction or nowcast was not possible for that bin because VIL could not be estimated.

Except Case 4, the model prediction is seen to be better than the advection-based nowcast under the criterion of r.m.s.e. Case 4, which occurred in late September, may not have been of convective nature though the daily weather map did not indicate any passing front. Also, it is noted that the characteristic radius R_c for Case 4 is conspicuously larger than the rest of the cases (see Table 1).

Examination of mean rainfall shows that the model tends to underpredict whereas the advection-based projection tends to overpredict. The main reason

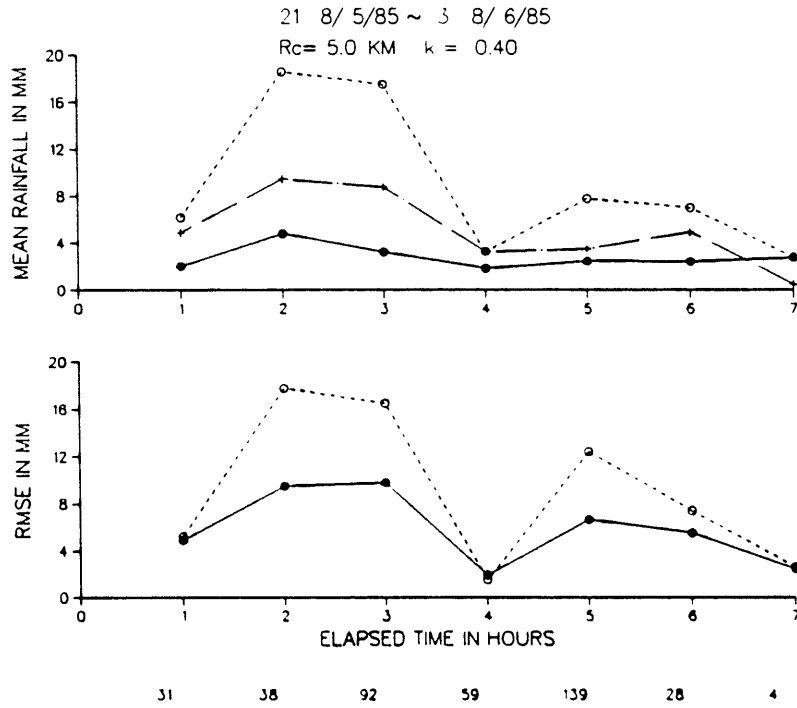


Fig. 9. Case 1 forecast comparison.

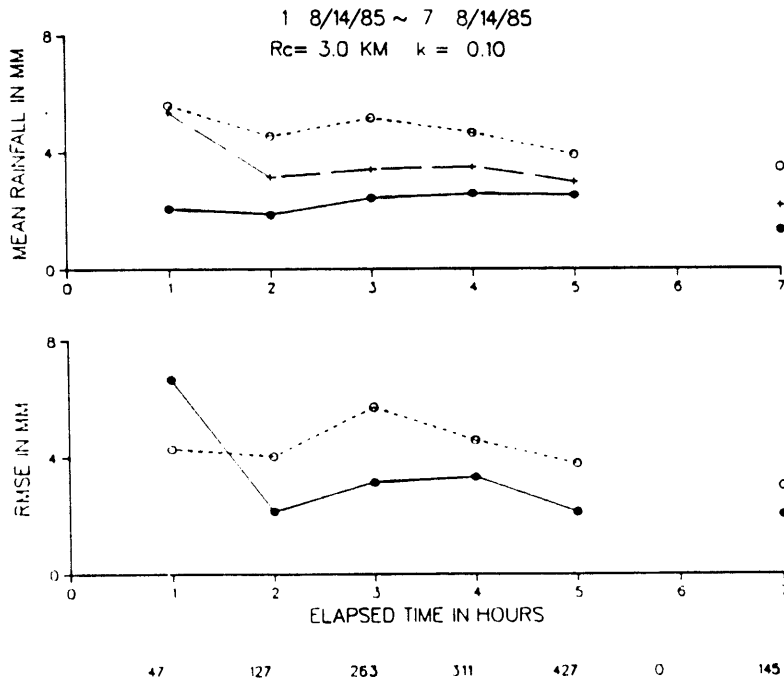


Fig. 10. Case 2 forecast comparison.

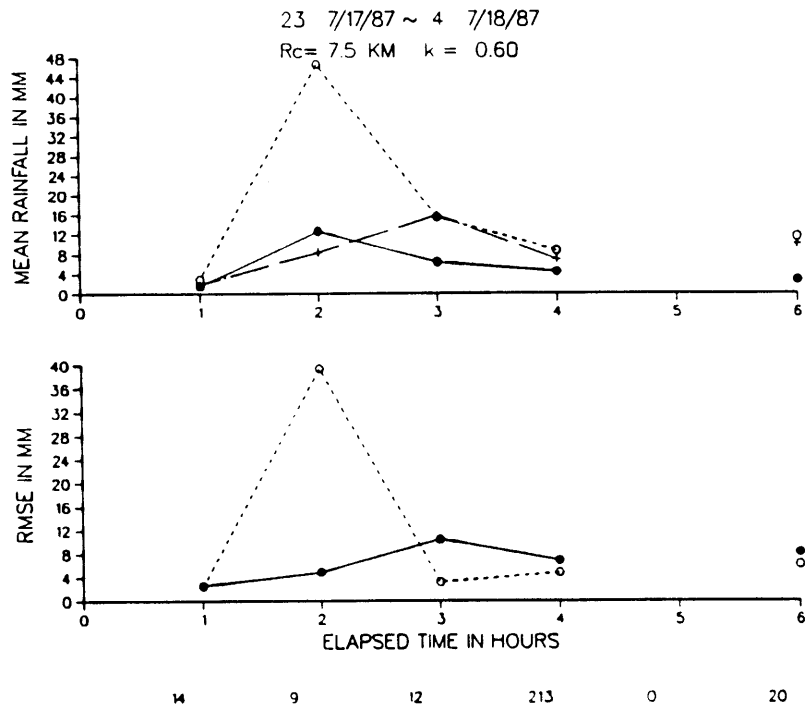


Fig. 11. Case 3 forecast comparison.

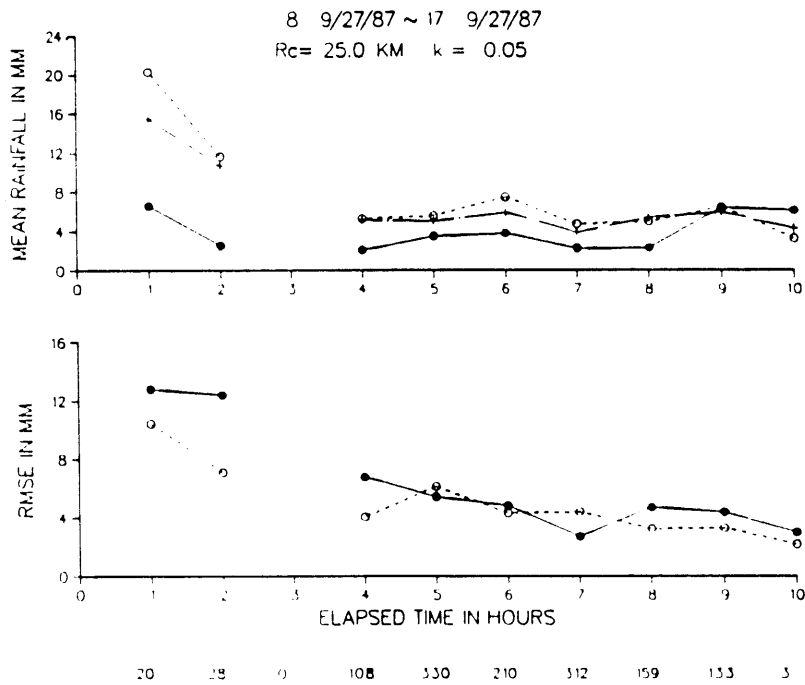


Fig. 12. Case 4 forecast comparison.

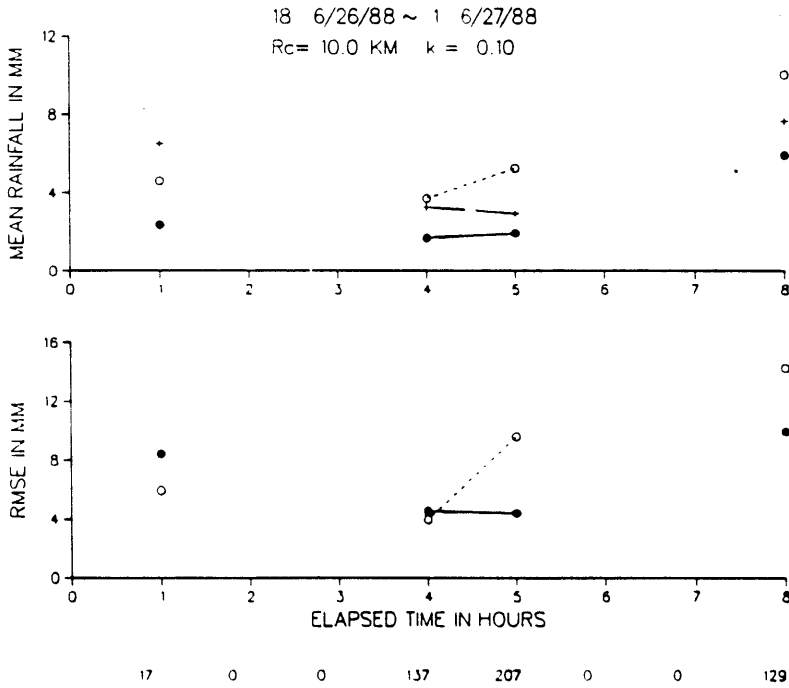


Fig. 13. Case 5 forecast comparison.

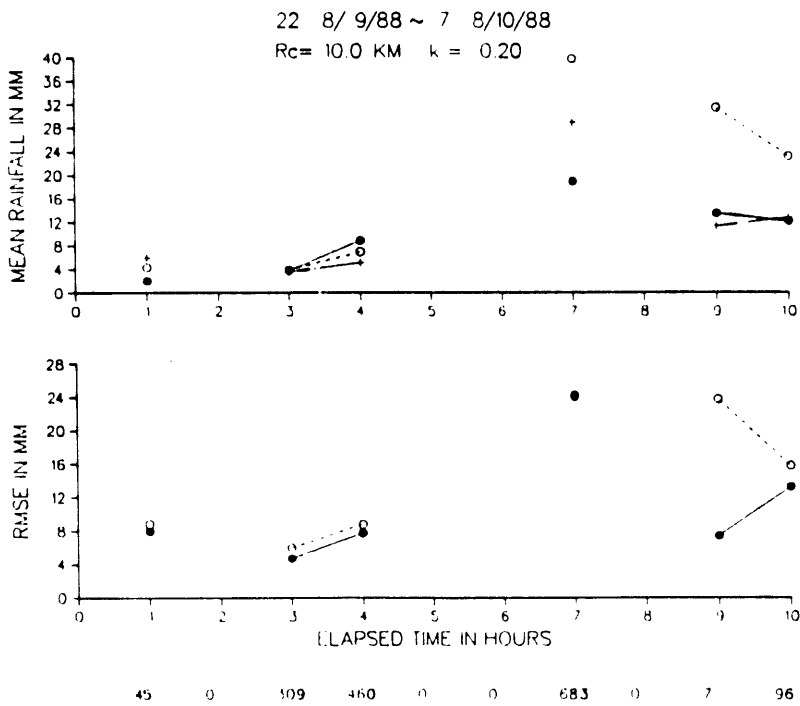


Fig. 14. Case 6 forecast comparison.

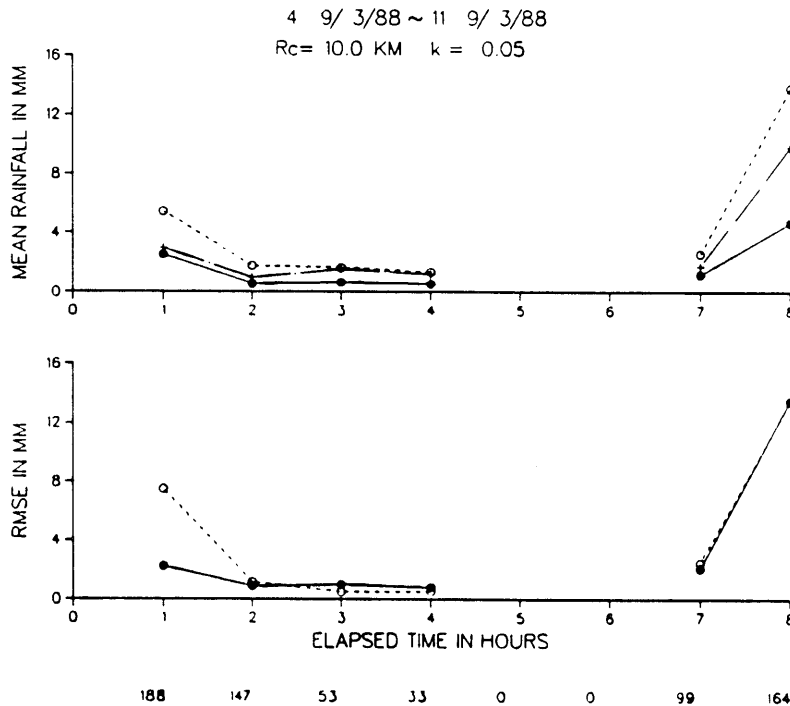


Fig. 15. Case 7 forecast comparison.

for the overprediction was traced back to the requirements on sample size and availability of higher vertical scans in estimation of VIL. The requirements tend to favor areas of short-lived bursts of very heavy rainfall but not areas of longer lasting light rainfall, thus resulting in overprediction. Many aspects of the model formulation can account for the apparent bias in the model prediction. Certainly some of the more limiting assumptions, such as instantaneous conversion of water vapor to rain water and constant echo-top height, contributed to the bias. One aspect of the model formulation that may be largely responsible for the bias is lack of explicit spatial averaging. The mass balance equations and momentum equations used in this work pertain only to a single cumulus column, and may introduce systematic biases when applied to a system of cumuli. A rigorous treatment of the issue (see, for example, Cotton, 1986), however, was beyond the scope of the modeling effort described in this work.

CONCLUSIONS AND FUTURE RESEARCH RECOMMENDATIONS

A radar-based short-term rainfall prediction model is described. The model is composed of a physically based component and a statistical component.

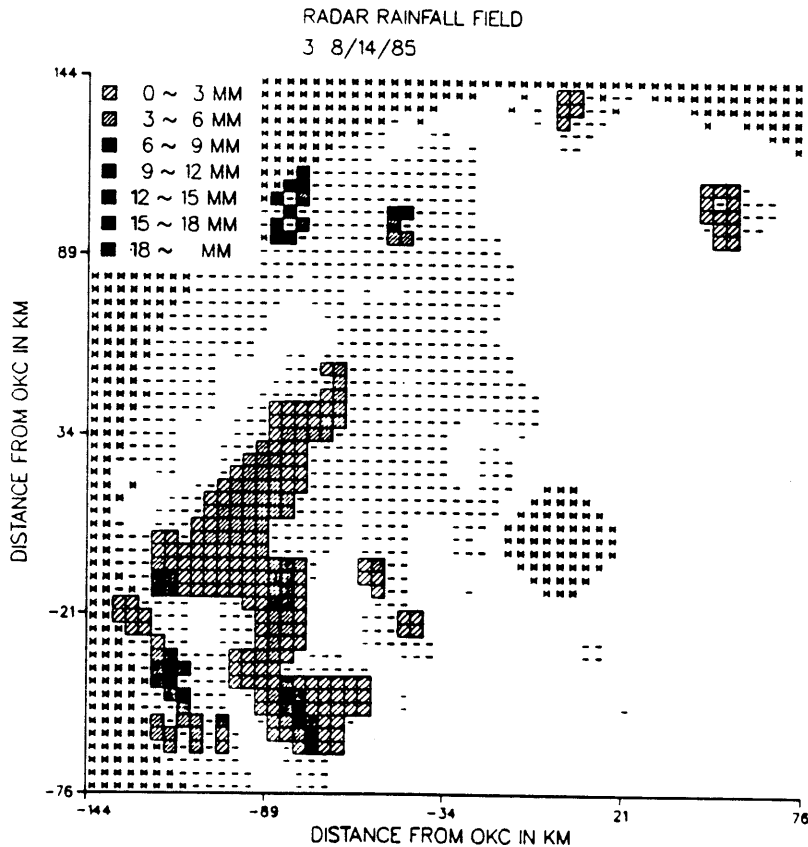


Fig. 16. An example of a radar rainfall field used as a true rainfall field.

The physically based part performs mass balancing of vertically integrated liquid water (VIL) to predict the mean VIL field, and the statistical part of the model performs prediction of residual VIL. The model is quasi-steady state in that conversion of predicted VIL to rainfall assumes constant echo-top height over the prediction lead time.

Owing to lack of data, an independent validation was not possible. Results from parameter estimation runs show that inclusion of the simple physical and statistical dynamics has potential in improving advection-based nowcasting under convective situations. To better evaluate the potential, however, much more extensive validation using, for example, data from the Next Generation Weather Radar System (NEXRAD) is necessary.

Model formulation and validation described in this work hinge on the validity of the Marshall-Palmer raindrop size distribution. Sensitivity of model performance on the M-P parameters needs to be examined.

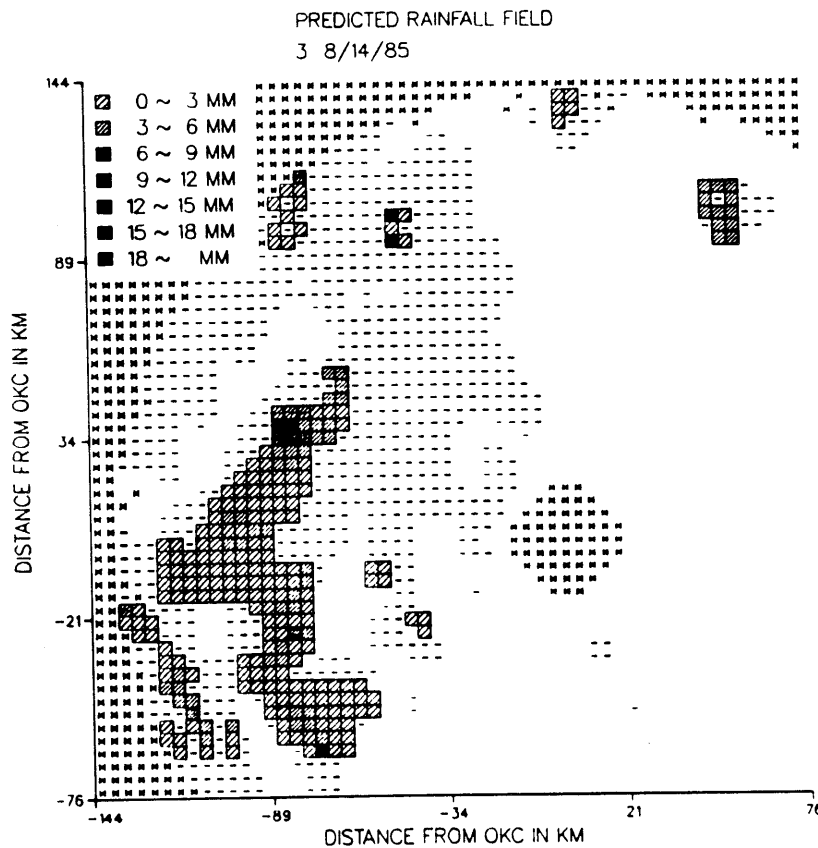


Fig. 17. An example of a model-predicted rainfall field.

Consequences of the assumptions such as instantaneous conversion of water vapor to rain water and constant echo-top height must be examined. It will help resolve issues such as vertical integration versus no vertical integration in physically based short-term rainfall prediction.

To be operationally useful, the two parameters, characteristic updraft radius (or, entrainment rate) and fractional constant, will have to be estimated in real time, or specified following some type of classification scheme.

Efforts should be made to utilize filtered or predicted fields from numerical weather prediction models, (for example, the Nested Grid Model (NGM) of the National Meteorological Center). In lieu of using radiosonde observations assuming persistence, one may use predicted fields from NGM. Owing to the difference in model terrain elevation and actual terrain elevation, however, temperature profiles near the surface as constructed from NGM output may be in severe disagreement with actual surface observations even over relatively flat areas (P. DiMego, personal communications, 1990).

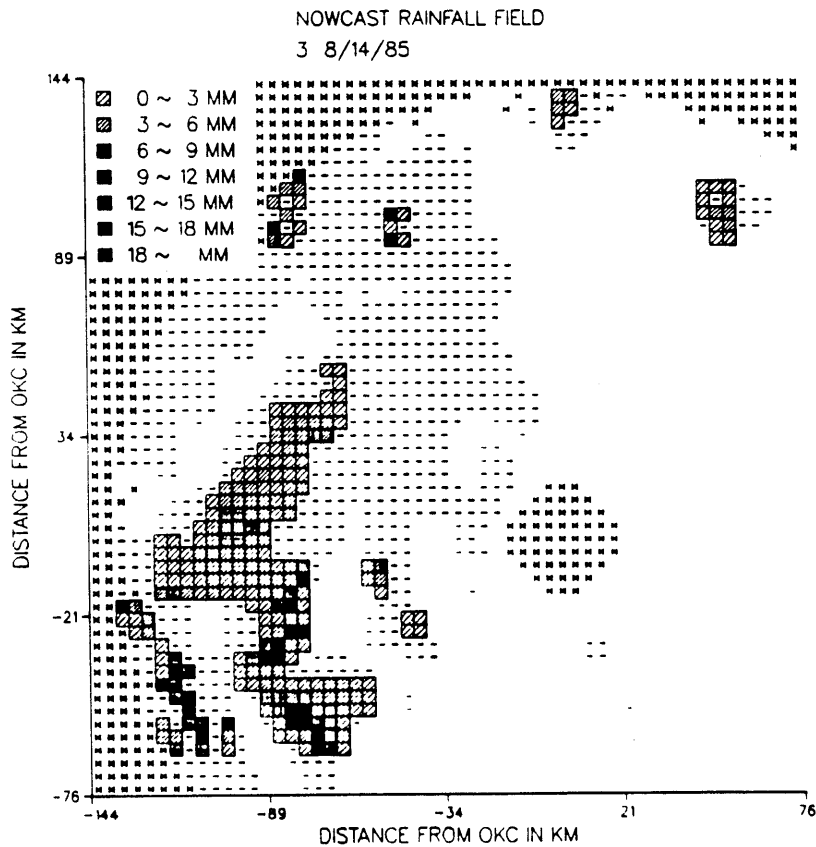


Fig. 18. An example of an advection-based nowcast rainfall field.

Eventually, the model formulation should be extended to use both radar and rain gage data, for example, in a distributed-parameter Kalman filter framework (Graham and McLaughlin, 1989). To do so, various types of error associated with VIL estimation must be identified and modeled.

Efforts must be made to include physical dynamics for frontal rainfall into nowcasting. Given that advection estimation procedures such as the maximum cross-correlation technique work better for frontal rainfall, physically based extension of advection-based nowcasting is better suited for frontal rainfall.

ACKNOWLEDGMENTS

This work was done while D.-J. Seo held a National Research Council-NOAA Research Associateship. J.A. Smith was supported in part by a research grant from the NEXRAD Joint System Program Office.

REFERENCES

- Anthes, R.A., 1977. A cumulus parameterization scheme utilizing a one-dimensional cloud model. *Mon. Weather Rev.*, 105: 270-286.
- Bellon, A. and Austin, G.L., 1978. The evaluation of two years of real-time operation of a short-term precipitation forecasting procedure (SHARP). *J. Appl. Meteorol.*, 17: 1778-1787.
- Bellon, A. and Austin, G., 1984. The accuracy of short-term radar rainfall forecasts. *J. Hydrol.*, 70: 35-49.
- Browning, K.A. and Collier, C.G., 1989. Nowcasting of precipitation systems. *Rev. Geophys.*, 27: 345-370.
- Browning, K.A., Collier, C.G., Larke, P.R., Menmuir, P., Monk, G.A. and Owens, R.G., 1982. On the forecasting of frontal rain using a weather radar network. *Mon. Weather Rev.*, 110: 534-552.
- Callahan, R.F., Short, D.A. and North, G.R., 1982. Cloud fluctuation statistics. *Mon. Weather Rev.*, 110: 26-43.
- Cotton, W.R., 1986. Averaging and the parameterization of physical processes. In: P.S. Ray (Ed.), *Mesoscale Models. Mesoscale Meteorology and Forecasting*. American Meteorological Society, Boston, MA, pp. 614-632.
- Dutton, J.A., 1986. *The Ceaseless Wind*. Dover, New York.
- Einfalt, T., Denolux, T. and Jacquet, G., 1990. A radar rainfall forecasting method designed for hydrological purposes. *J. Hydrol.*, 114: 229-244.
- Elvander, R.C., 1976. An evaluation of the relative performance of three weather echo forecasting techniques. In: Preprint Vol. 526-532 of the 17th Conf. on Radar Meteorology, Seattle. AMS, Boston.
- Georgakakos, K.P. and Bras, R.L., 1984a. A hydrologically useful station precipitation model 1. Formulation. *Water Resour. Res.*, 20: 1585-1596.
- Georgakakos, K.P. and Bras, R.L., 1984b. A hydrologically useful station precipitation model 2. Case studies. *Water Resour. Res.*, 20: 1597-1610.
- Graham, W. and McLaughlin, D., 1989. Stochastic analysis of nonstationary subsurface solute transport 2. Conditional moments. *Water Resour. Res.*, 25: 2331-2355.
- Greene, D.R. and Hudlow, M.D., 1982. Hydrometeorologic grid mapping procedures, presented at AWRA Int. Symp. on Hydrometeorology, Denver, CO, 13-17 June. American Water Resources Association, Bethesda, MD.
- Gunn, R. and Kinzer, G.D., 1949. The terminal velocity of fall for water droplets in stagnant air. *J. Meteorol.*, 6: 243-248.
- Gupta, V.K. and Waymire, E., 1988. Short contribution on Taylor's hypothesis and dissipation in rainfall. Technical Note, Utah Water Resources Lab., Utah State University, Logan.
- Hess, S.L., 1979. *Introduction to Theoretical Meteorology*. Robert E. Krieger, Huntington, New York.
- Huff, F. and Vogel, J., 1981. Real-time rainfall monitoring-prediction system and urban hydrology applications. *J. Water Resour. Plann. Manage.*, WR2: 419-435.
- Johnson, E.R. and Bras, R.L., 1980. Multivariate short-term rainfall prediction. *Water Resour. Res.*, 16: 173-185.
- Kessler, E., 1969. On the continuity of water substance in atmospheric circulations. *Meteorol. Monogr.* 10, No. 33, 84 pp.
- Leese, J.A., Novak, C.S. and Clark, B.B., 1971. An automated technique for obtaining cloud motion from geo-synchronous satellite data using cross-correlation. *J. Appl. Meteorol.*, 10: 118-132.

- Marshall, J.S. and Palmer, McK., 1948. The distribution of raindrops with size. *J. Meteorol.*, 5: 165-166.
- Pielke, R.A., 1984. *Mesoscale Meteorological Modeling*. Academic, Orlando, FL.
- Pruppacher, H.R. and Klett, J.D., 1978. *Microphysics of clouds and precipitation*. Reidel, Hingham, MA.
- Reuter, G.W., 1990. Radar observations of precipitation production in thunderstorms. *Atmos. Ocean.*, 28: 216-229.
- Saffle, B. and Greene, D., 1978. The Role of Radar in the Flash Flood Watch Warning System — Johnstown Examined. 18th Conf. on Radar Meteorology, Atlanta, GA. American Meteorological Society, Boston, MA.
- Seo, D.-J. and Smith, J.A., 1991. Rainfall estimation using rain gages and radar — a Bayesian approach: 2. an application. *Stoch. Hydrol. Hydraul.*, 5(2): 31-44.
- Simpson, J. and Wiggert, V., 1969. Models of precipitating cumulus towers. *Mon. Weather Rev.*, 97: 471-489.
- Smith, J.A. and Krajewski, W.F., 1991. Estimation of the mean field bias of radar rainfall estimates. *J. Appl. Meteorol.*, 30: 397-412.
- Walton, M.L. and Johnson, E.R., 1986. Proposed on-site flash flood potential system for NEXRAD. Preprints, 6th Conf. on Hydrometeorology. AMS, Boston, pp. 122-129.

